

Tidal Flow Around Obstacles

Kristen Thyng

December 7, 2007

Abstract

Flow around obstacles is a complex topic which many researchers are working on. Stratified tidal flow is a specific subset of this topic which has specific issues and complications to work around. This paper reviews two articles about distinct but related flows around obstacles in the Pacific Northwest. Each paper compares measurement data with either model output or theory and analyzes the data, working toward a better understanding of geographic flows.

1 Introduction

Researchers have been interested in flow around obstacles for a long time. It is a topic of interest for local physical oceanographers and geophysical fluids dynamicists in the Pacific Northwest since one of the most striking features of the local geography is the Puget Sound, a fjord with complex topography. As computing power has increased, many doors have been opened to researchers as far as their ability to tackle new and exciting tasks to learn more about the details of flow about obstacles. In this process, two of the many papers in recent years are to be discussed in this review paper: *Form Drag and Mixing Due to Tidal Flow past a Sharp Point*, by Edwards et al (2004), and *Stratified Tidal Flow over a Bump*, by Dewey et al (2005).

The first examines a model created by Lavelle et al in 1988 of the Puget Sound. In it, the researchers needed to use a quadratic drag coefficient of $1-2 \times 10^{-2}$ in order to match measured data. This is much higher than is normally needed. Edwards et al propose that it is higher because it is taking into account not only frictional drag but also form drag, which is increased because of the rough topography. In order to investigate the phenomena, the authors arrange for observational data around Three Tree Point (TTP), a large, sloping ridge that extends out into the Puget Sound. In addition, a numerical simulation is created using the hydrostatic Hallberg Isopycnic Model (HIM).

The second paper seeks to compare previous lab experiments and research with measurements made off the southern tip of Vancouver Island near a bump in the seabed. Dewey et al first lead readers through expected flows due to a range of topographic Froude numbers, then present the data and work out what may be occurring.

This review paper will first address the paper by Edwards et al with a summary followed by analysis and comments. The second half of the paper will do the same for the paper by Dewey et al.

2 Tidal Flow Past a Sharp Point

The authors use Puget Sound geographic feature Three Tree Point (TTP, see Figure 1) in order to investigate the kinetic energy conversion process between barotropic tidal current into mixing areas and turbulence. As tides come into coastal areas, they meet bathymetric features that may be of sufficient height to affect the flow and remove a significant amount of kinetic energy. In the case of TTP, tides collide with a prominence from the land that extends into the waterway. These collisions cause enhanced mixing of the stratified flow and three-dimensional turbulence. The bathymetric features lead to further mixing of the stratified water within the turbulent boundary layer. This removal of energy can be quantified by the free-stream velocity times the area-integrated boundary stress. This boundary stress can be further broken down into frictional stress from the bottom boundary layer and form drag due to pressure differences across topographic features.

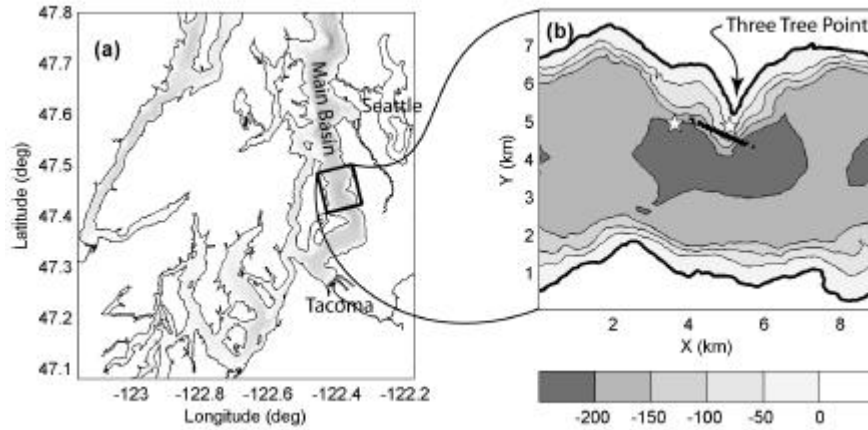


Figure 1: Map of the location of Three Tree Point (TTP) (b) and its location in the Puget Sound (a). Note that (b) also shows the path of the ship taking measurements as well as the location of two bottom-mounted ADCP units (shown as stars).

Edwards et al explain the intricacies of form drag. They differentiate between ‘internal form drag’, which is caused by the deformation of isopycnals in stratified flow, and ‘external form drag’, which is caused by deformation of the sea surface. In the case at hand, two mechanisms can produce this form drag, at both the surface and underwater: flow separation and wave generation. These mechanisms have similar pressure consequences (high pressure upstream, low pressure downstream), but in the former higher flow velocities are found upstream whereas in the latter they are found downstream.

Few measurements on form drag have been made because of the difficulty of measurements in the water column, particularly involving an underwater obstacle. For this reason, the authors looked to numerical simulation in their research.

2.1 Equations

The authors express the boundary drag as follows:

$$D = D_{\text{BBL}} + D_{\text{FORM}}^{\text{int}} + D_{\text{FORM}}^{\text{surf}},$$

where D_{BBL} is the frictional drag due to the bottom boundary layer in the direction of the section integrated over that section, $D_{\text{FORM}}^{\text{int}}$ is the internal form drag, and $D_{\text{FORM}}^{\text{surf}}$ is the external form drag. The internal form drag is calculated from

$$\frac{D_{\text{FORM}}^{\text{int}} + D_{\text{FORM}}^{\text{surf}}}{W} = - \int_{X_1}^{X_2} p_B \frac{d\zeta}{dx'} dx',$$

where W is the width of the bump, p_B is the pressure at the ocean bottom, $d\zeta/dx'$ is the along-section topographic slope, and the endpoints X_1 and X_2 have the same bottom depth. The external form drag cannot be calculated from the measurements and is instead calculated outside of this paper. The pressure term related to the internal form drag can be calculated as follows (making the assumption that the flow is hydrostatic):

$$p_B^{\text{int}} = \int_{\zeta}^{z_0} g\rho dz.$$

The frictional drag was calculated in a more complicated manner. The authors started out assuming the relationship $\tau_0 = \rho u_*^2$ in the log layer, where u_* is the friction velocity. The rate of turbulent kinetic energy production and the mean shear $\partial U/\partial z$ can be related by $-\overline{u'w'}/\partial z = \varepsilon$, where $-\overline{u'w'}$ is the vertical Reynolds stress and is equivalent to u_*^2 . Using the ‘law of the wall’ relation, $\partial U/\partial z = u_*/kz$ with k as the von Kármán constant, we find

$$u_* = (\varepsilon kz)^{1/3}.$$

The final estimate for the frictional drag is made by averaging approximations to ε above the bed with the assumption they were in the log layer, averaging along the track between X_1 and X_2 , and then finding the desired number per unit area by multiplying by $|X_1 - X_2|$ and dividing by H_T , the height of the obstacle.

2.2 Measurements

In nine crossings over TTP, a ship measured flow properties using a vertical profiler called Chameleon, which was developed at Oregon State University. The device was sent down approximately every 107 meters and took data from the sea surface to the seabed, though the top 10 meters were thrown out due to disturbance from the ship’s wake. The device measured temperature, conductivity, and approximate turbulent dissipation rate. The ship also carried an Acoustic Doppler Current Profiler (ADCP) which was used to take current measurements over the side of the ship, of which 10 meters at the top of the water column and the bottom 15% of the water column were thrown out due to contamination. Two ADCP units were moored to the seabed to record currents from a fixed location. See Figure 1 for these locations.

The timing of the surveys is marked on the tidal currents, U_T , with respect to time, as seen in Figure 2. This figure also shows other relevant information about the physical occurrences

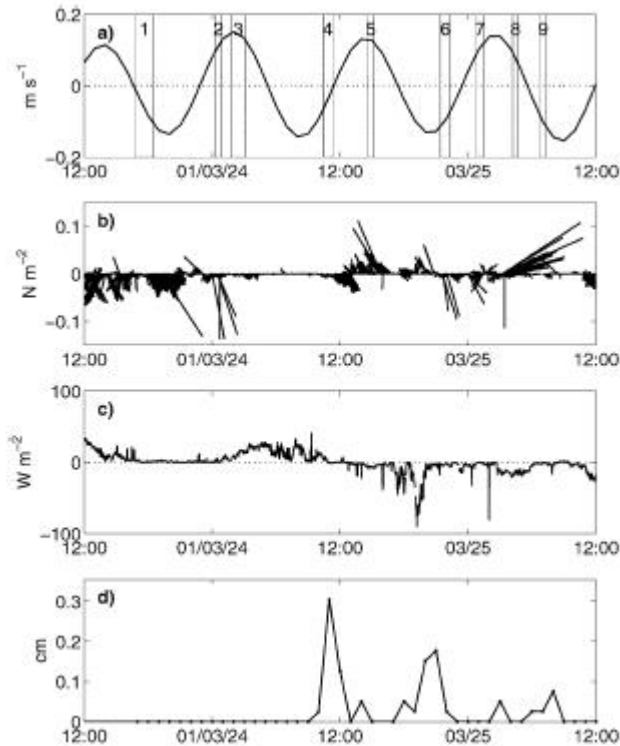


Figure 2: Conditions during the surveys: (a) Predicted tidal currents U_T with the surveys marked appropriately, (b) wind stress vectors (Note that a storm came in around noon on March 24), (c) sum of the sensible and latent heat fluxes on the ship, and (d) hourly precipitation.

during the surveys, such as wind stress, sensible and latent heat fluxes, and hourly precipitation. The figure of wind stress shows that a storm came in around noon on March 24, affecting measurements. One of the major effects from the environment during the surveys was a near doubling in stratification in the upper 20 meters of the water column due to the storm.

An examination of the surveys finds a couple of trends. One trend found the isopycnals around the bump to dip downstream, strongest during the strong tides, with a bunching-up of density on the upstream side, relax in between, and then do the same thing when the tide switched direction. The dip was strongest on the downstream side with steepest descent of the rock-face. Around the time period of maximum flood, steep downward velocities were found in the dip followed by similar upward velocities downstream in a relatively short horizontal distance, leading the authors to suspect a standing lee wave combined with a headland eddy. They also note that the eddy diffusivity values were high in the isopycnal dip.

A possible reason for differing flow in response to the obstacle was discussed in an earlier paper by MacCready and Pawlak (2001). They found that the flow takes the shortest path over a sloping ridge when $Fr_{\text{slope}} > 0.5$ but will take a more horizontal path when $Fr_{\text{slope}} < 0.5$ and travel around the ridge, which corresponds loosely to a flow that has strong stratification.

MacCready and Pawlak defined Fr_{slope} as follows:

$$Fr_{\text{slope}} = U_T [LN \sin(a)]^{-1}.$$

This interpretation helps the authors reason that this is a probable reason for the behavior of the flow at strong tides. They found that at maximum flood, when the conditions cause less stratification, the flow went over the bump, causing the formation of a lee wave, whereas when it was more stratified, the flow went around.

2.3 Model

Since measurements allow the researchers to calculate the desired drags only in two-dimensions, it is necessary to create a numerical model to attempt to calculate these parameters in three-dimensions. The setup is such that the results will be at best qualitative in that a reentrant channel was artificially created to simplify the problem and avoid the need for open boundary conditions. The authors assert that this not a terrible approximation because the scales in the domain (see Figure 1(b)) are great enough that the eddies to be examined are unlikely to be affected for at least a few tidal cycles.

The code used for this simulation is the hydrostatic Hallberg Isopycnic Model (HIM). The turbulence parameterization used was Richardson number-dependent, giving the rate of turbulent entrainment through an interface as

$$w_e = \begin{cases} \Delta u \frac{0.1-0.1\text{Ri}}{1+5\text{Ri}} & \text{Ri} < 1 \\ 0 & \text{Ri} \geq 1, \end{cases}$$

where Δu is the velocity difference across layers and Ri is the bulk Richardson number,

$$\text{Ri} = \frac{g'h}{\Delta u^2}.$$

In this equation, we find the reduced gravity, $g' = g\Delta\rho/\rho_0$, where $\Delta\rho$ is the density step across an interface and h is the average thickness of adjacent layers. The resolution of the model is 100 meters horizontally and 20 isopycnal layers of 12 meter thickness. This model uses z -coordinates, rather than terrain-following coordinates, leading to the need to calculate the bottom stress using a quadratic drag law with coefficient $C_D = 2.5 \times 10^{-3}$, since the bottom boundary layer is not well resolved in this type of coordinate. This coefficient comes from averaging the interpolated velocity over the bottom 15 meters. A realistically-sized boundary layer is created as the bottom stress is distributed upward in the water column by diapycnal fluxes.

The model is forced inasmuch as to recreate a tidal velocity, U_T , previously predicted by Lavelle et al (1988). The forcing takes into account only U_T , an along-channel tidal velocity, because there is no net across-channel transport and thus no across-channel forcing. The desired current is appropriately split amongst six tidal constituents, M_2 , S_2 , N_2 , K_1 , O_1 , and P_1 , and the along-channel body force is calculated to implement the desired forcing. The model was run for 216 lunar hours (12.42/12 hours) starting from rest.

2.4 Model-data comparison

As can be seen in Figure 3, the model is able to simulate the general features of the flow at TTP, but it does not capture many of the details. For example, the tidal cycle timing is close, but the peaks often do not line up on the along-channel currents. Much of the modeled currents also do not line up in the across channel velocities, particularly near the top of the ridge. The authors reason that these are off because even a small error in the bathymetry in the model will throw off the separation point in the flow from TTP. One major observation that can be taken from both the model and the data is the evidence of flow separation, as seen by the consistent negative velocities in the across-channel flow near the top of the ridge, as seen in Figure 3, in the left-side figure.

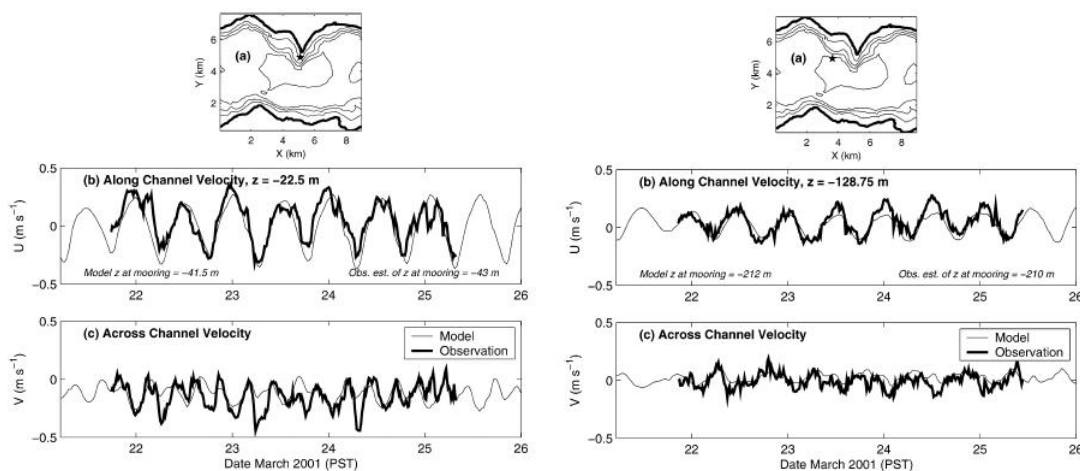


Figure 3: Comparison between the model output and observed data from the moored ADCP units. On the left is the comparison at middepth near the top of the ridge, location shown in (a). Also shown in the along-channel velocity (b) and the across-channel velocity (c). Similar figures are seen on the right for the comparison at middepth away from the ridge.

As far as drag is concerned, there is some reasonable comparison. The authors plot the form drag and frictional drag separately versus time because the form drag is much higher than the frictional drag. See Figure 4 for the comparison. One place in particular that the model underpredicts the form drag is at the third star, which corresponds to a point at which the model was not able to reproduce the large downwelling of light surface water in a lee wave, which would have effected the drag.

The authors use their study to help explain a previous result found by Lavelle et al (1988). Lavelle modeled the Puget Sound and needed to greatly raise the friction parameter in his model in order to accurately simulate the tides. Edwards et al offer a possible explanation. They reason that the friction parameter needed to be greater because of form drag effects in the flow. Since the authors actually found that the frictional drag was quite low, the logical explanation is that Lavelle raising the friction accounted for the form drag that was not present in his model. The authors continue by stating the importance of form drag in mixing in the

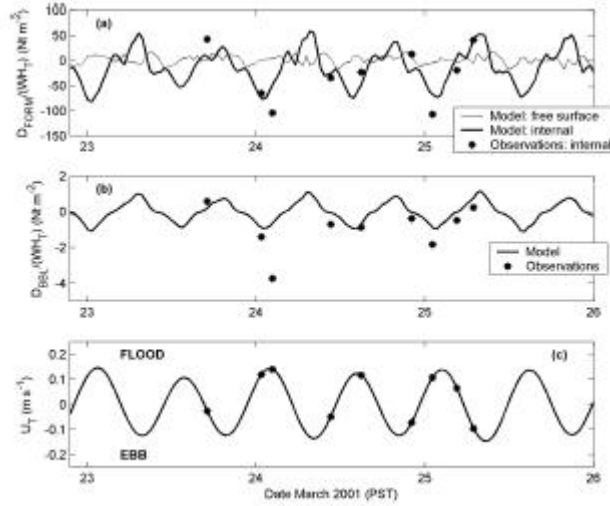


Figure 4: Comparison of model output for form drag (a) and frictional drag (b) per unit frontal area versus time, and a plot to show the timing relative to U_T (c).

Puget Sound. Classic boundary layer drag enhances mixing, but only near the topography, whereas form drag is found to enhance mixing in an area on the order of the full depth of the water column and a great volume. These disturbances thus can greatly affect the flow in addition to leading to important consequences for mixing issues.

2.5 Conclusions

Edwards et al present what appears to be a significant insight into flows in the Puget Sound. Researchers increasingly look toward numerical modeling to understand complex flows, and this is a good example of these models, along with appropriate data, coming together to further our collective knowledge. The more closely simulations can model reality without ad hoc adjustment of parameters to make numbers match, the more we will in turn be able to learn.

Good modeling was accomplished in this research because of the insight attained. However, the model is highly idealized, with many liberties having been taken along the way. They artificially create a reentrant channel to avoid open boundaries. This appears to not created a significant problem based on the large size of the model domain in comparison to the range of the eddies to be examined, but the more realistic a model can be run, the more the results can be trusted.

The researchers also use a hydrostatic model. This assumption greatly simplifies the modeling and computational time. It is worth noting that it may be a weak assumption in this case. As discussed, the flow around TTP can be highly turbulent and unstable. When this is the case, the flow is generally not hydrostatic. The observational data shows evidence of a lee internal wave, which is fast-moving in the vertical direction. This behavior is non-hydrostatic, and as expected, is not resolved by the numerical simulation.

In view of the ideas presented in this paper, it makes sense to follow up with more measurements to test the theories and continue to tune our understanding. Improving the model by moving

to a non-hydrostatic model would help to match data with model output so that the model could provide insight of its own.

3 Flow Over a Bump

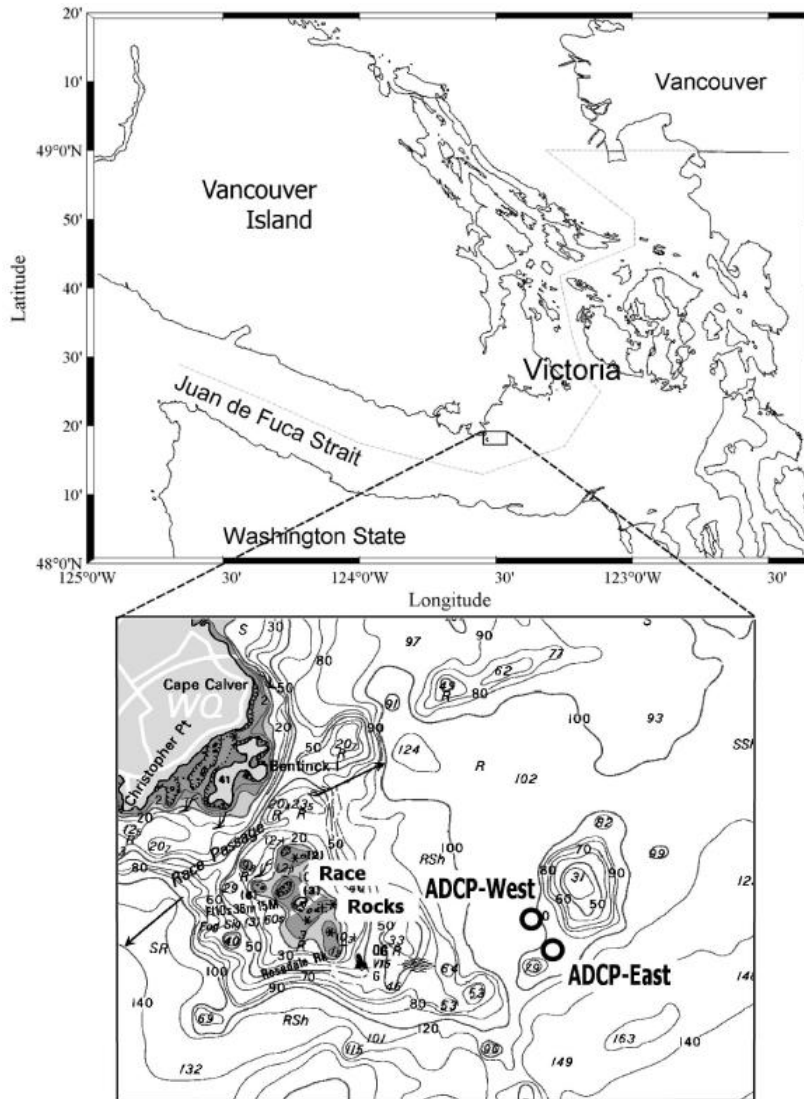


Figure 5: Map showing the area of interest.

Dewey et al propose an examination of an obstacle by looking first at what may be expected from previous lab data around an ‘ideal’ bump, then using equipment to take in data in order to compare the two. The area to be examined is just off the southern end of Vancouver Island (see Figure 5). This bump has a height of around 70 meters in water that is about 100 meters deep and it has steep sides. It is close to ideal in that it is approximately symmetric. The tides in the area are mixed semi-diurnal, and the bathymetry leading up to the bump from the

northeast is relatively flat, whereas from the Race Rocks side it is uneven. Since the ebb tides approach the bump from the northeast where the bathymetry is more favorable for isolating the effects of the bump on the flow, the measuring equipment, to be discussed later in this paper, was placed on the lee side of the bump during ebb tide, thus on the southwest side (see Figure 5).

3.1 Parameters

Dewey et al explain in their paper that the topographic Froude number is likely to be the most important nondimensional number in this flow. This Froude number is defined as

$$F = \frac{U}{Nh}, \quad (1)$$

where U is the upstream velocity, N is the buoyancy frequency given by $N^2 = -g/\rho(\partial\rho/\partial z)$, and h is the height of the bump. From previous studies, Dewey et al approximate the strong and relatively uniform stratification in the area to be $N \approx 1.1 \times 10^{-2} \text{ s}^{-1}$. Then, given that the bump height is estimated as 70 meters, the Froude number can be approximated by

$$F = \frac{U(t)}{0.77}.$$

For anticipated currents from 0.25 to 1.5 m/s^{-1} , Dewey et al then expect the range of Froude number to be 0.33 - 1.95 (lower speeds are generally not seen because the tidal cycle traces out an ellipse and the flow is never truly still). Lower Froude number typically corresponds to a mostly two-dimensional flow. An increase in the Froude number toward 1 sees an increase in vertical velocities as well as the start of internal lee waves. As the Froude number increases beyond 1, the wake becomes three-dimensional.

The authors do compare the significance of the Froude number with some other nondimensional parameters. For example, they point out that h/H , where H is the water depth, is only important when it is close to 1, whereas in this case h/H is approximately $.7$ and the authors expect little effect on the free surface flow. They also say that the parameter $\omega L/U$, where L is the half-width of the bump, is important in that it dictates whether a quasi-steady state will be reached during the tidal cycle so that internal waves and other disturbances will have time to develop (it will in this case because this parameter is small).

3.2 Expectations

It makes sense to start with an examination of flow over an ideal bump in stratified flow. Starting with a Froude number of around 0.2 , Dewey et al expect horizontal flow separation around the obstacle, but limited vertical flow deviation, especially above the obstacle. They would expect the wake to include vortical modes or alternating eddies.

Allowing the Froude number to increase up to approximately 0.5 , Dewey et al expect to see the beginnings of movement in the flow ahead of the obstacle that is approximately the same height as the bump, with increases specifically in the vertical displacement of flow. This increase in vertical displacement ahead of the flow would also correspond to an increase after the flow,

along with the development of wake and boundary mixing, both vertically and horizontally. The flow that is approximately the same height as the bump will travel up over the bump, then accelerate down the opposite side. Flow that is further below the top of the bump will not have enough momentum to make it all the way over the bump and will instead separate around the obstacle horizontally.

As the Froude number increase to 1.0, the behavior found in the previous situation will be much more pronounced; flow ahead of the bump will have stronger vertical displacement and more of the flow will make it over the top of the bump, then accelerate downward on the lee side, forming an internal wave. The fast moving flow may even form a hydraulic jump, and the free surface flow may be affected.

As the Froude number increases to be greater than 1.0, one may expect to find that the internal wave that had been developing on the lee side of the bump will break loose and flow downstream. Flow will be mostly vertical instead of horizontal. The wake will grow in size as well as develop a reduced pressure drop, and as shears grow there will be increased turbulence and mixing.

See Figure 6 for images of flow expectations.

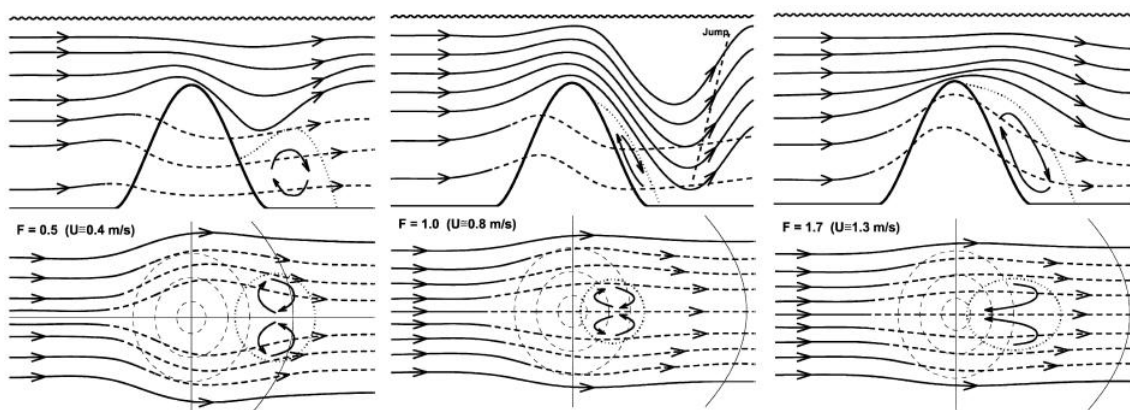


Figure 6: These images show streamlines from a variety of sample Froude numbers ranges. The top image in each shows a vertical cross-section while the bottom shows a horizontal cross section. The far left image is for $F \approx .5$, the center is for $F \approx 1$ and the right for $F > 1$.

Since the focus of this paper is on the reality of tidal flows, particular in the Puget Sound, it is important to put this flow in context. The flow will be going through all the tidal phases over time, thus each of these situation may be encountered throughout a single day as the flow goes from slack tide to flood tide. Also, as the flow goes from slack tide to ebb tide, the flow will reverse direction and the lee side of the bump will be, instead, the side of approach for the flow. This, along with the fact that the flow may deviate from the direction of flow depending on the tide as well as the tidal cycle (*i.e.* the tides may not be exactly bidirectional), implies that the situation will be always changing and possibly difficult to predict. If the flows change too quickly, a quasi-steady state may never be attained, in which case none of this analysis

would apply.

3.3 Measurements

Measurements were made in order to investigate flow over a real bump just off Vancouver Island. Two Acoustic Doppler Current Profilers (ADCPs) were mounted on the seabed, with placements as seen in Figure 5, and one ADCP was brought on a ship in order to take over-the-side measurements. The bottom-mounted ADCPs were left underwater for approximately four days in order to obtain data from multiple M_2 tidal cycles. The over-the-side measurements from the ship were accomplished during ebb tide and involved repeated tracks over the bottom-mounted ADCPs and the bump.

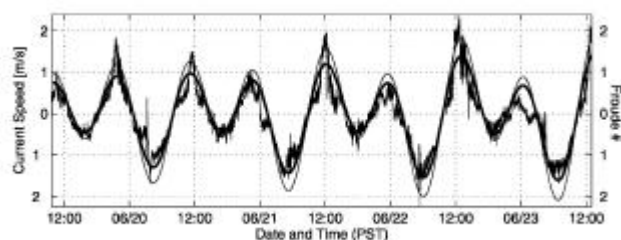


Figure 7: Velocities measured by the easterly ADCP, averaged over height interval 60-70m are shown by the squiggly line, predicted tidal currents U_{tide} taken from a regional barotropic tidal model are shown by the thicker line, and $F = U_{\text{tide}}/0.77$ is shown by the thin line.

The mixed semidiurnal tides are shown in Figure 7 as taken from the ADCP-east unit, along with a current prediction from a regional tidal model and the Froude number. It is possible to clearly see both the weak and strong ebb and flood tides.

3.4 Analysis

Dewey et al found it most appropriate to subdivide the analysis of the observations by Froude number, analogously to earlier in the paper when describing flow expectations. This makes sense since a wide range of Froude numbers was represented by the tidal flow around the bump. The first section to discuss would then be subcritical flows, for flows with a Froude number value below 1. Note that despite the possibility that the tidal cycle and situation being examined may not allow for enough time for any sort of coherent structures to appear in the flow, as mentioned in the expectation section, analysis found that indeed the tidal flows over the bump can be considered quasi-steady.

Subcritical flows were examined by Dewey et al by looking specifically at the weak ebb tide. Looking at Figure 7, the maximum Froude number in ebb tide is around 0.7, placing the weak ebb tide solidly in subcritical flow and expectations to align with the previously discussed ideal case when the Froude number is approximately 0.5. Indeed, certain aspects of this flow does match with its expectation. Flows above the bump are found to be relatively unaffected. The more westerly ADCP unit is downstream of the right side of the bump, when viewed from

upstream during ebb tide, and this unit is found to have some flow inward toward the bump. This possibly indicates a region of low pressure from the wake. The more easterly ADCP unit is directly behind the bump when viewed from upstream. This unit finds rotary shears and some vertical velocities, as one would expect from a mixing wake region. Because the flows in ADCP-east are directed mostly west, Dewey et al decide that this unit is on the eastern flank of the wake area, making the wake area wide (effecting both ADCP units) and thus consistent with the expectations. Despite previous findings that Dewey et al reference, they did not see evidence at this lower Froude number of coherent eddy shedding on the lee side of the bump.

The critical flow is interesting in particular because it lends itself well to comparing the three regions of Froude number together, as the flow changes from subcritical to critical, then pushes beyond to supercritical. As expected, Dewey et al found the currents above the bump to be effected by the fast flow. When the Froude number was approximately equal to 1, during the strong ebb tide, Dewey et al were able to detect the development of a lee wave with the easterly ADCP unit. However, there was no evidence of this lee wave in the westerly ADCP-unit, despite its relatively close proximity. According to the authors, the lee wave develops in the area between the bump and the easterly ADCP unit as the flow becomes critical. As the flow becomes supercritical, the lee wave is swept downstream and thus into the range of ADCP-east. The first traces of the lee wave would be its tail into ADCP-east, as evidenced by strong upward velocities in the upper water column, which were seen, followed by the progression of the vertical velocities down the water column, then horizontal velocities, and finally downward velocities throughout the column, starting at the base. This motion was seen in the flow. The westerly ADCP unit saw possible evidence of being on the edge of the lee wave, as expected since the unit was on the edge of the wake. See Figure 8 for an artistic interpretation of what may be happening.

Also to be investigated in the critical flow is the possibility of a hydraulic jump. Evidence of such a structure can be found by examining the difference between the four transducer faces in the ADCP unit. These faces are obviously close together and generally ‘see’ approximately the same flow. In this case, there was a slight difference between the transducers that is consistent with the passing of a very fast, steep disturbance that is too quick to be an internal wave. Immediately afterward, the disturbance had passed. This was then followed by the lee wave.

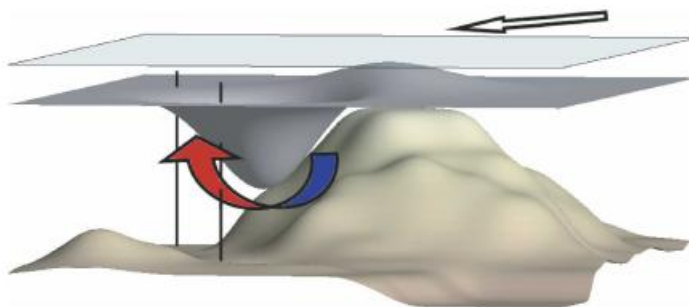


Figure 8: A possibility for flow behavior that is seen in data.

Supercritical flow finds strong currents in the flow, looking at peak strong ebb tide. The upper water column is highly effected by the bump, showing strong currents as well. There is strong shearing in the flow since, for example, at the westerly ADCP unit, below the more uniform upper water column, there is a section of strong downward velocities. The easterly ADCP unit shows shear in the upper water column, upward velocities in the middle of the column, and a boundary layer at the bottom. This asymmetrical behavior is not what was sketched out earlier in the paper, possibly because this bump is not perfectly symmetric nor smooth, as assumed. Another point is that Dewey et al expected to see the return of the lee wave upon switch of the tidal direction, though it is often seen in two-dimensional examples. A possible explanation of this is that the lee wave in this example is very three-dimensional and may have missed the two ADCP units and over-the-side measurements. The authors suggest further study to pursue this idea.

3.5 Conclusions

As stated in this paper, there is not enough data to know much of this analysis very certainly. It is difficult and costly to gather data, but more stationary ADCP data would certainly aid in the analysis process. For example, it would be worthwhile to validate the theory that the lee wave is not seen to return because of too little data available. In addition, knowledge gained at this location could be checked in other local areas to attempt to find a consensus. Edwards et al also find evidence of a lee wave in their observational data. The knowledge gained by each respective party can be combined and expanded upon.

As seen in the first paper, modeling can be used to help put pieces of analysis together. Future work for Dewey's group could be to create a numerical simulation that is able to match the creation of the internal lee wave in the critical Froude number range. Once this is accurately accomplished, the group may be able to track its movement around the tidal cycle to see why it was not picked up a second time by the ADCP units.

4 Conclusion

There are many researchers working on problems in tidal flows around obstacles. This paper has reviewed two recent papers on the subject: flow past a sharp point and flow over a bump. It is clear that progress is being made by the combined use of theory, lab experiments, numerical simulation, and observation. Such insights gained continue to improve human understanding of the world and should continue to be pursued.

References

- [1] Dewey, R., D. Richmond, and C. Garrett, 2005: Stratified Tidal Flow over a Bump. *J. Phys. Oceanogr.*, **35**, 1911-1927.
- [2] Edwards, K. A., P. MacCready, J. N. Moum, G. Pawlak, J. M. Klymak, and A. Perlin, 2004: Form drag and mixing due to tidal flow past a sharp point. *J. Phys. Oceanogr.*, **34**, 1297-1312.

- [3] Lavelle, J. W., H. O. Mofjeld, E. Lempriere-Doggett, G. A. Cannon, D. J. Pashinski, E. D. Cokelet, L. Lytle, and S. Gill, 1988: A multiply-connected channel model of tides and tidal currents in Puget Sound, Washington and a comparison with updated observations. NOAA Tech. Memo. ERL PMEL-84 (PB89-162515), 103 pp.
- [4] MacCready, P., and G. Pawlak, 2001: Stratified flow along a corrugated slope: Separation drag and wave drag. *J. Phys. Oceanogr.*, **31**, 2824-2839.